

Supporting Information

In situ Synthesis of Bi₂O₃/Bi₂S₃ Composite Heterojunction for the Electrochemical Characterization of Supercapacitors

1. Experimental Section

1.1 Electrochemical testing

The loads of the symmetrical and asymmetrical capacitors are calculated from Equation S1:

$$\frac{m^+}{m^-} = \frac{C^- \Delta V^-}{C^+ \Delta V^+} \#(s1)$$

where m+ and m- represent the mass of the positive and negative electrodes, respectively, C (F g-1)

is the specific capacitance, and ΔV (V) is the discharge voltage range.

2. DFT Calculation

2.1 Differential Charge Calculation

The density functional theory calculations were carried out by the Vienna Ab initio simulation package (VASP)^{24, 25} based on the projected augmented wave (PAW) method, in which the exchange correlation energy is described by the functional of Perdew, Burke, and Ernzerhof (PBE) scheme²⁶ including the van der Waals (vdW) dispersion van der Waals corrections (DFT-D3 method)²⁷. The cutoff energy of the planewave basis set was set at 500 eV. The convergence criterion was less than 10⁻⁵ eV in energy, 0.05 eV Å⁻¹ in force. The Brillouin zone integrations were performed by using Monkhorst Pack 2×2×1 for geometric optimization. To avoid periodic interactions, all models had a vacuum layer greater than 15 Å.

The band, density of states, figure of merit, and adsorption energy calculations were carried out using the CASTEP module of the MS2018 modeling and simulation package, and the Perdew Burke Ernzerhof (PBE) function from the Generalized Gradient Approximation (GGA) method was used to describe the

exchange-correlation potential. The plane wave cutoff energy is 450 eV, and the Brillouin region is geometrically optimized using a $2 \times 2 \times 1$ K point grid. SCF tolerance: 2.0×10^{-6} eV atom $^{-1}$.

The adsorption energy is calculated as:

$$E_{ads} = E_{slab + molecule} - E_{slab} - E_{molecule}$$

where E_{ads} is the adsorption energy, $E_{(slab+molecule)}$ is the total energy after adsorption, and E_{slab} and $E_{molecule}$ represent the substrate energy and the energy of the adsorbed substance, respectively.

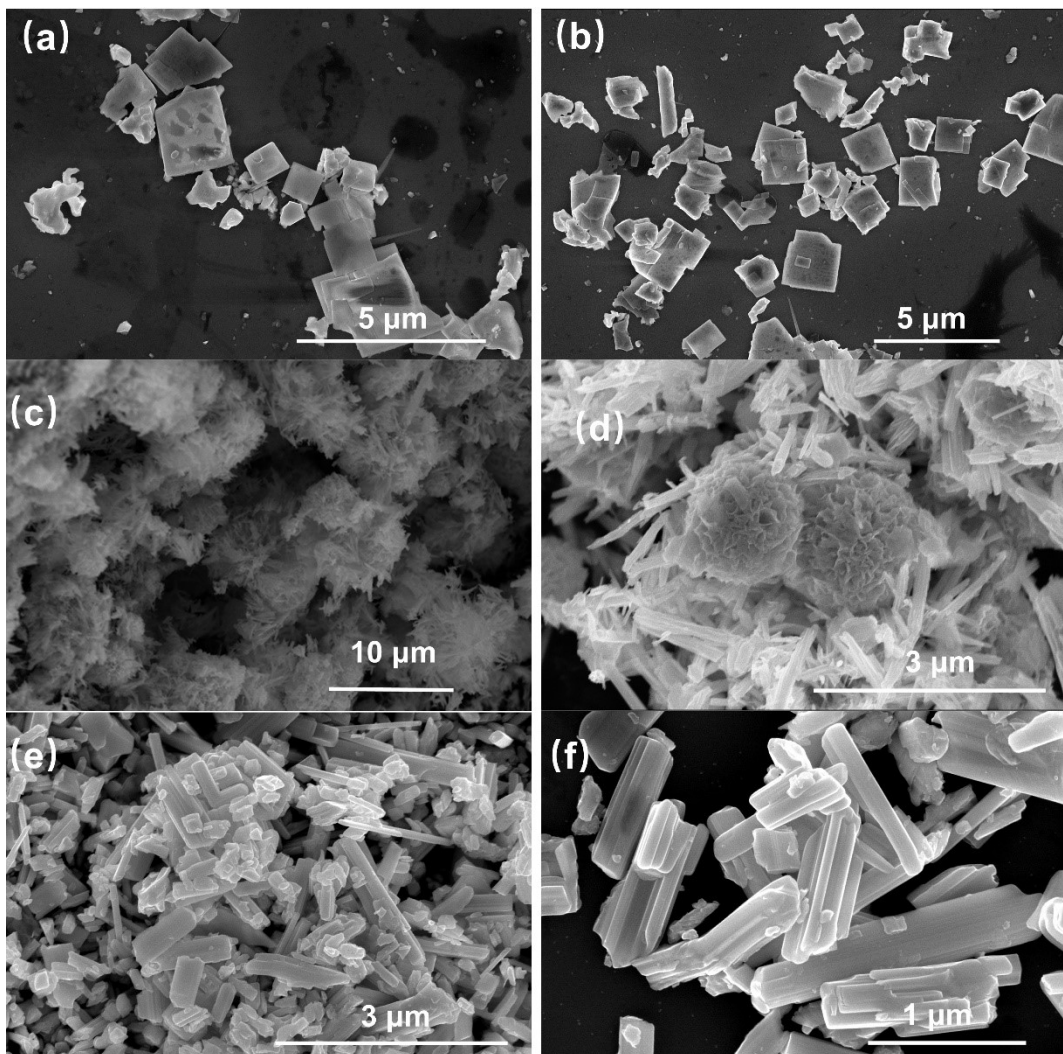


Fig. s1 (a-b) SEM images of BO; (c-d) SEM images of BS; (e-f) SEM images of BO/BS; (g) SEM images of BO-attached nickel foam; (h) SEM images of BS-attached nickel foam; (i) SEM images of BO/BS-attached nickel foam; (j) empty nickel foam SEM

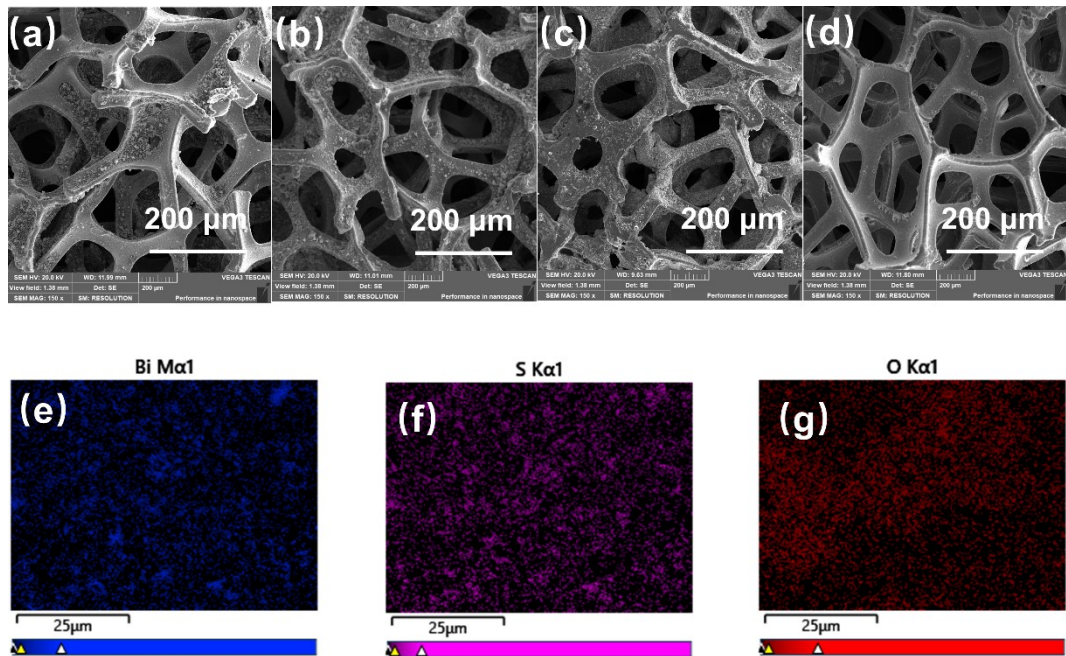


Fig. S2 (a) SEM image of BO-attached nickel foam; (b) SEM image of BS-attached nickel foam; (c) SE M image of BO/BS-attached nickel foam; (d) SEM image of empty nickel foam; (e-g) EDS images of B O/BS

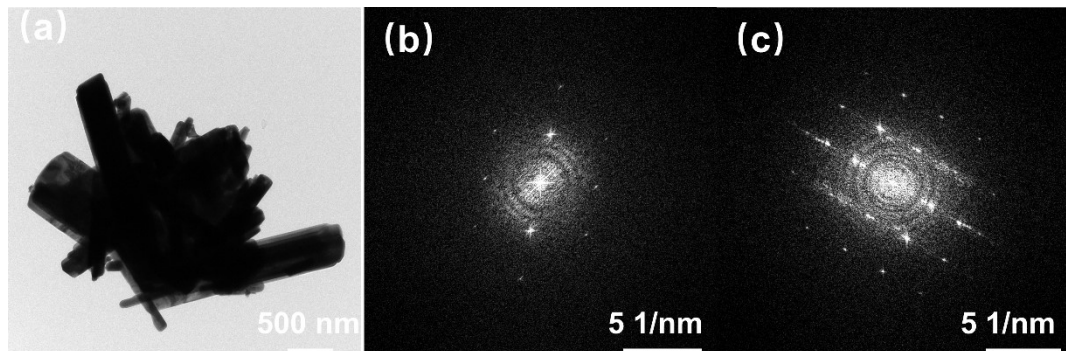


Fig. S3 (a) TEM image of BO/BS; (b-c) SAED images of BO/BS samples

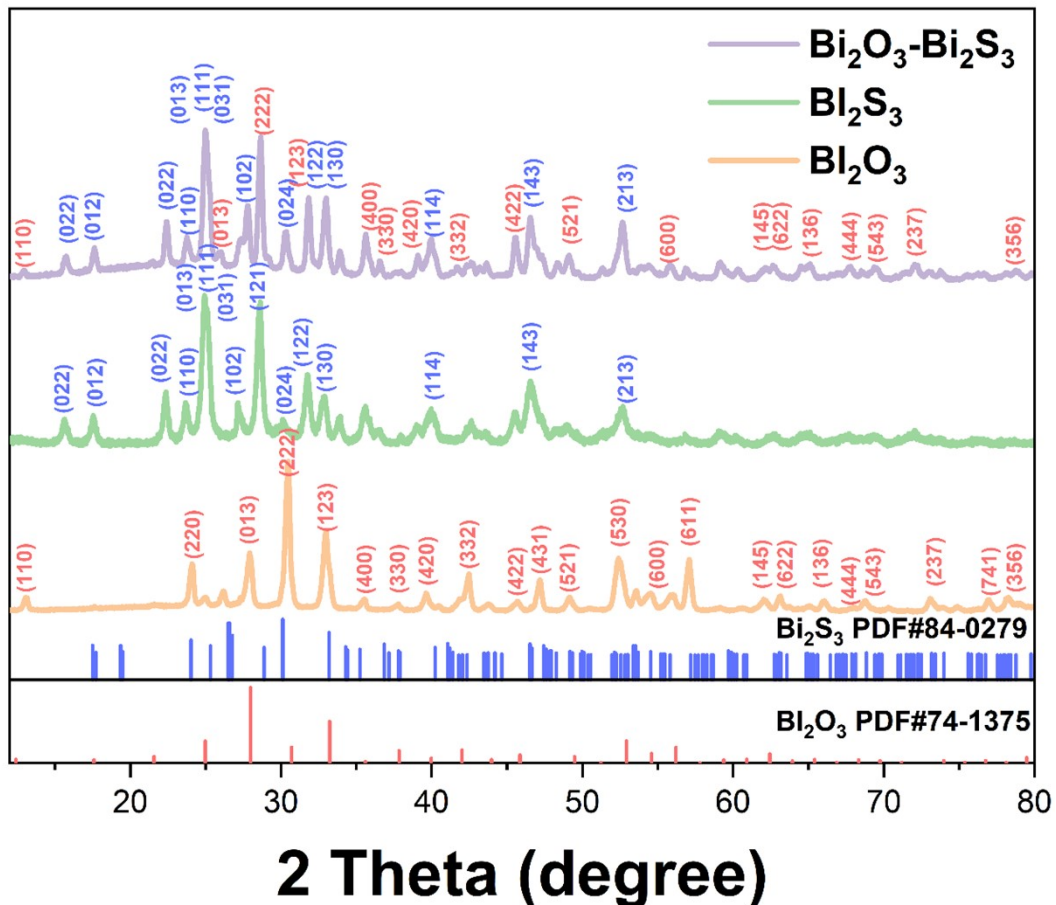


Fig. S4 XRD of BO, BS, BO/BS

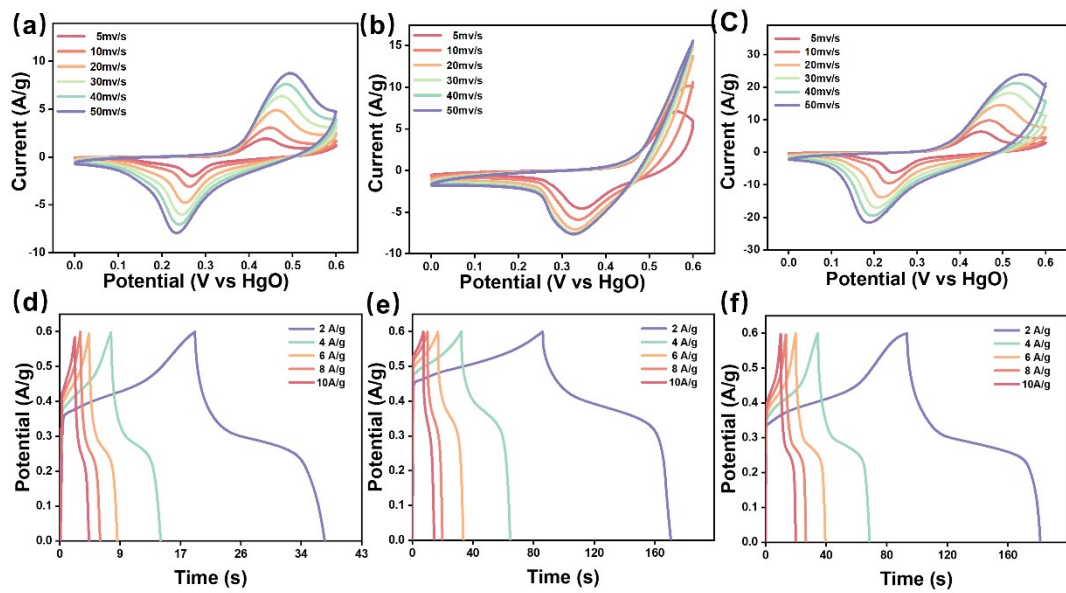


Fig. S5 (a) CV curve of BO; (b) CV curve of BS; (c) CV curve of BO/BS;(d) GCD curves of BO; (e) GCD curves of BS; (f) GCD curves of BO/BS;

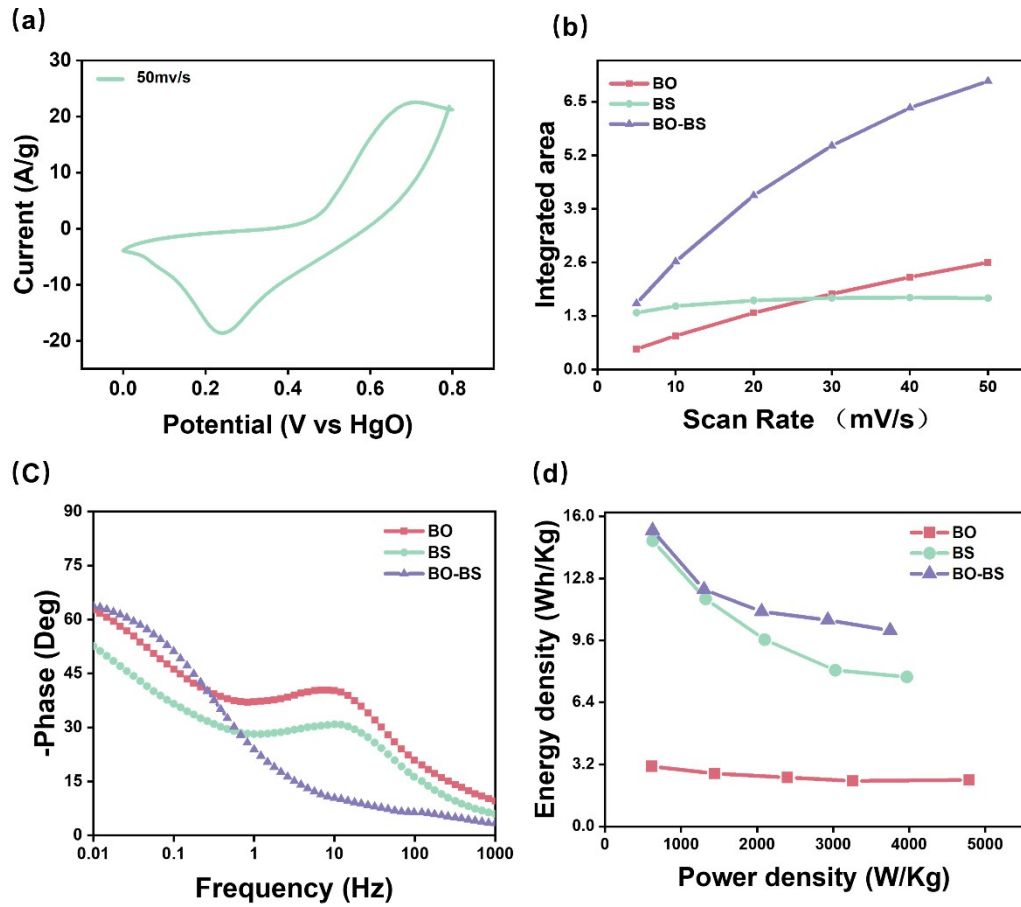


Fig. S6 (a) CV curves of BS at 0-0.8 V; (b) Integral areas of BO, BS, and BO/BS with respect to CV;
(c) Porter phase angles of BO, BS, and BO/BS; (d) Ragone plot

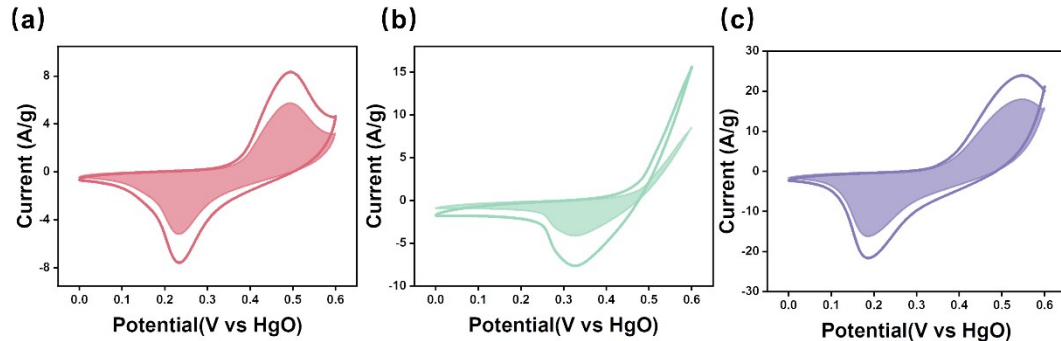


Fig. S7 Diffusion control occupancy at 50 mV s⁻¹ sweep rate (a) CV curve of BO; (b) CV curve of BS;
(c) CV curve of BO/BS

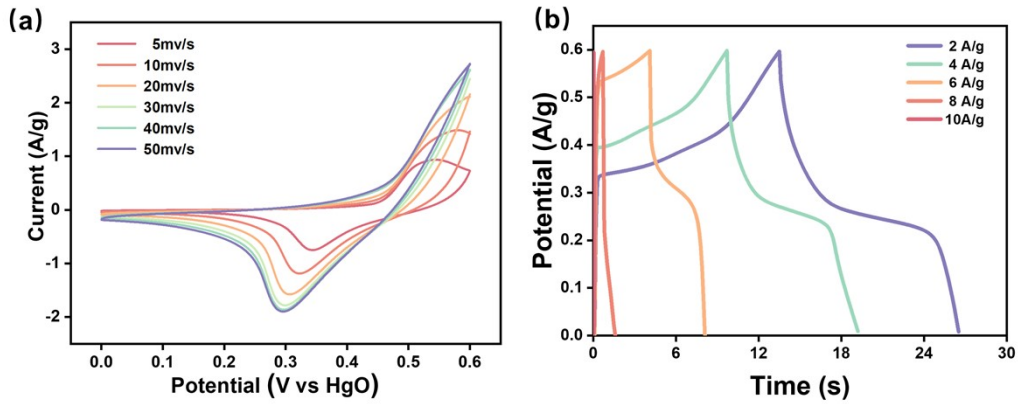


Fig. S8 Electrochemical performance of the physically mixed BO and BS sample, (a) Cyclic Voltammetry (CV) and (b) Galvanostatic Charge-Discharge (GCD) curves.

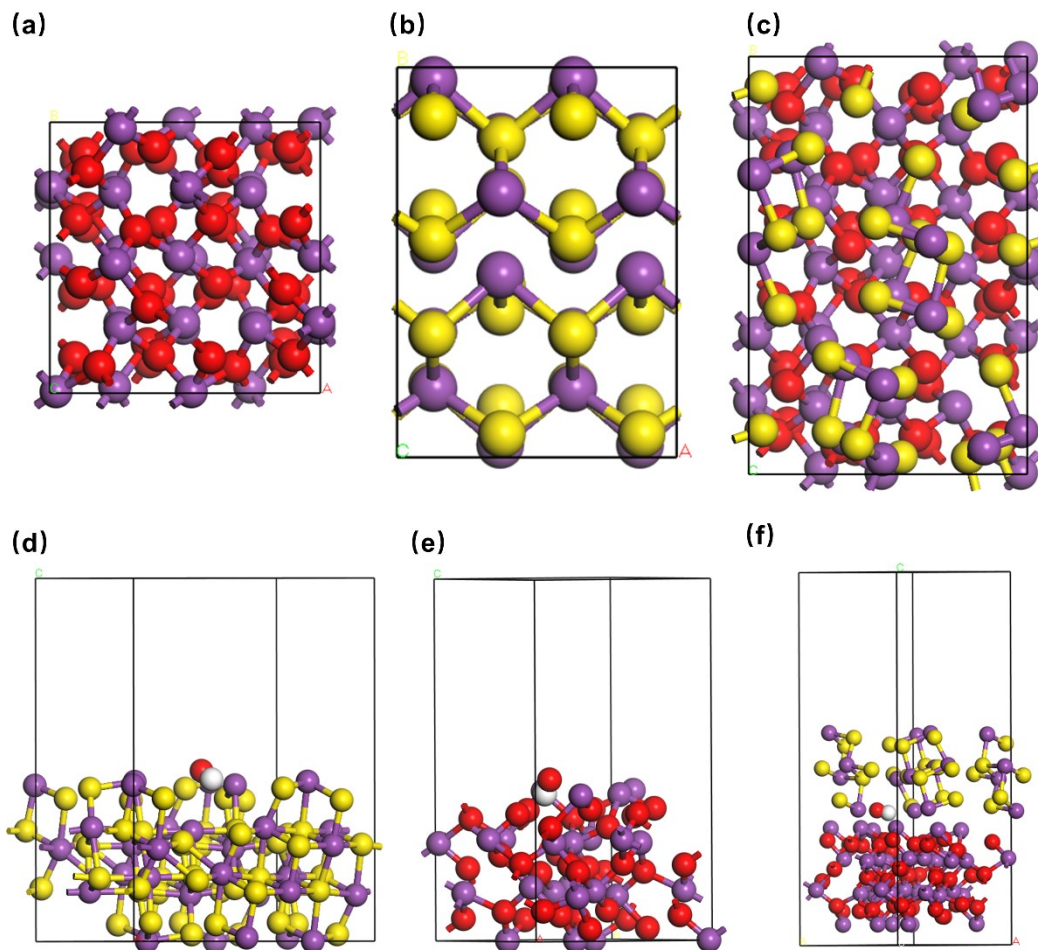


Fig. S9 (a) Top view of the Bi_2O_3 model; (b) Top view of the Bi_2S_3 model; (c) Top view of the $\text{Bi}_2\text{O}_3/\text{Bi}_2\text{S}_3$ model; (d) Model of the $\text{Bi}_2\text{O}_3(2\ 0\ 0)^1$ facet; (e) Model of the $\text{Bi}_2\text{S}_3(1\ 3\ 0)^1$ facet; ;(f) Model of the $\text{Bi}_2\text{O}_3/\text{Bi}_2\text{S}_3$ heterojunction after faceting

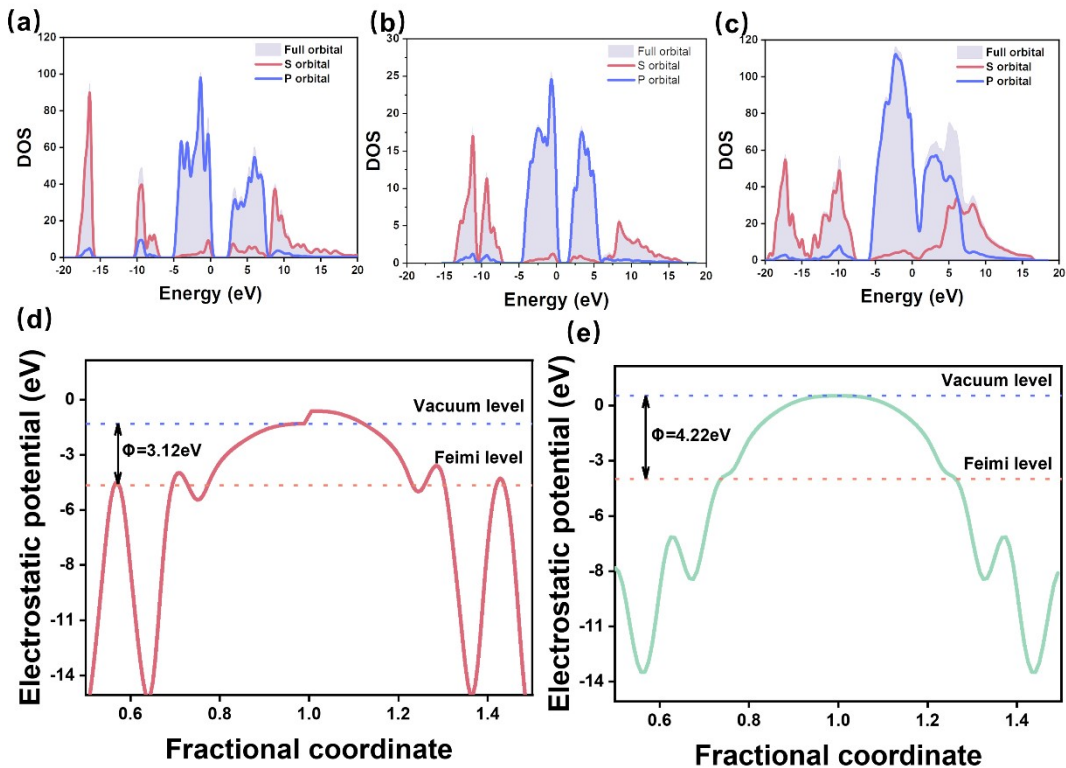


Fig. S10 (a) DOS plot of Bi_2O_3 ; (b) DOS plot of Bi_2S_3 ; (c) DOS plot of $\text{Bi}_2\text{O}_3/\text{Bi}_2\text{S}_3$; (d) Work function calculation of Bi_2O_3 ; (e) Work function calculation of Bi_2S_3

Sample	SBET (m ² g ⁻¹)	Pore volume (cm ³ g ⁻¹)	Average pore size (n m)	C value	linear factor
BO	0.4040	0.00025	2.42766	32.72859	0.99812
BO/BS	1.7360	0.00094	2.16106	12.72628	0.99989

Tab.S1: BET testing of BO, BO/BS

The lattice parameters	BO	BS	BO/BS
a (Å)	10.08906	4.387	7.2688
b (Å)	10.08906	11.147	8.639
c (Å)	10.08906	11.305	11.9698
effective lattice constant	$\sqrt{305.364}$	$\sqrt{271.188}$	$\sqrt{270.882}$
α (°)	90	90	87.713
β (°)	90	90	93.227
γ (°)	90	90	86.653

Tab.S2: Lattice parameters of BO, BS, BO/BS

Scanning speed rate (m V s ⁻¹)	SBO	SBS	SBO/BS
5	0.497	1.378	1.604
10	0.816	1.537	2.618
20	1.373	1.674	4.224
30	1.833	1.733	5.432
40	2.239	1.745	6.351
50	2.598	1.730	7.001

Tab.S3: Integral area of BO, BS, BO/BS with respect to CV

Sample (A g ⁻¹)	2	4	6	8	10
BO	62.0	54.5	50.6	47.1	47.8
BS	294.8	235.4	194.5	161.6	154.4
BO/BS	305.6	246.2	221.8	213.0	202.8

Tab.S4: Specific capacitance of BO, BS, BO/BS at different capacitance densities

Scanning speed rate (m V s ⁻¹)	BO	BS	BO/BS
5	12.72%	7.78%	9.67%
10	16.14%	11.86%	12.16%
20	20.84%	20.00%	16.44%
30	24.93%	29.17%	19.45%
40	28.22%	37.84%	22.60%

50

31.13%

45.45%

24.75%

Tab.S5: Surface control ratios of BO, BS, and BO/BS at different sweep speeds

Scanning speed rate (m V s ⁻¹)	BO	BS	BO/BS
5	87.28%	92.22%	90.33%
10	83.86%	88.14%	87.84%
20	79.16%	80.00%	83.56%
30	75.07%	70.83%	80.55%
40	71.78%	62.16%	77.40%
50	68.87%	54.55%	75.25%

Tab.S6: Diffusion control ratios of BO, BS, and BO/BS at different sweep speeds

	BO	BS	BO/BS
Rs	0.8205	0.77429	0.78511
Rct	9.168	1.417	0.023808
CPE1-T	0.023284	0.032391	0.0029713
CPE1-P	0.72358	0.89192	1.215
Wo-R	1.156	17.17	1.741
Wo-T	0.035505	7.953	50594
Wo-P	0.36607	0.45658	0.36788

Tab.S7: Fitted circuit parameters for BO, BS, BO/BS

materials of the heterojunction	adsorbed species	adsorption energy (eV)
carbon ²	SBP ⁺	-3.36
MoS ₂ in-planes ³	NH ₄ ⁺	-2.49
P-doped NiO ⁴	OH ⁻	0.64
NiCo ₂ S ₄ ⁵	OH ⁻	-3.0654
CuCo-LDH/BPQD ⁶	OH ⁻	0.375
This work	OH ⁻	-7.66

Tab.S8: Comparison of Adsorption Energies

Sample	Potential window	Electrolyte	Specific capacitance	Stability
Bi ₂ S ₃ /MWC ⁷	-0.6~0V	0.5 M Na ₂ SO ₄	133 F g ⁻¹ (1 A g ⁻¹)	80 %(3000 cycles,10 A g ⁻¹)

Bi ₂ O ₃ /porous-RGO ⁸	-1.2-0.2V	6 M KOH	243 F g ⁻¹ (5 mV s ⁻¹)	81.1 %(3000cycle,0.5 A g ⁻¹)
PEDOP/Bi ₂ S ₃ ⁹	-0.2-0.8 V	organic electrolyte	201 F g ⁻¹ (1 A g ⁻¹)	94 %(1000 cycle,1 A g ⁻¹)
Bi ₂ Se ₃ @C ¹⁰	-1.1-0V	6 M KOH	540 C g ⁻¹ (2 A g ⁻¹)	90.5 %(1000 cycle,1 A g ⁻¹)
Ag/Bi ₂ O ₃ /g-C ₃ N ₄ ⁶	0.2-0.6V	KOH	100.5 Fg ⁻¹ (2 A g ⁻¹)	
Flowerlike Bi ₂ MoO ₆				
Hollow Microspheres ₁₁	0-0.6V	3 M KOH	182 Fg ⁻¹ (1 A g ⁻¹)	80 %(3000 cycle,5 A g ⁻¹)
Bi ₂₅ FeO ₄₀ +7 wt %P VP ¹²	-1-0V	6 M KOH	232 F g ⁻¹ (4 A g ⁻¹)	84 %(1000 cycle,5 A g ⁻¹)
Bi ₂ S ₃ /FGS ¹³	-0.9-0V	1 M Na ₂ S _{O₄}	292 F g ⁻¹ (1 A g ⁻¹)	75 %(5000 cycle,5 A g ⁻¹)
MoS ₂ /Bi ₂ S ₃ ¹⁴	-0.2-0.8V	1 M KOH	120 Fg ⁻¹ (1 A g ⁻¹)	87.7 %(2000 cycle,1 A g ⁻¹)
Bi ₂ S ₃ /graphene ¹³	-0.9-0V	1 M Na ₂ S _{O₄}	292 F g ⁻¹ (1 A g ⁻¹)	75 %(5000 cycle,5 A g ⁻¹)
BiFeO ₃ ¹⁵	0-0.45V	3 M KOH	253 F g ⁻¹ (1 A g ⁻¹)	88 %(5000 cycle,10 A g ⁻¹)
Bi ₂ WO ₆ /rGO HGs ¹⁶				
			268.7 F g ⁻¹ (0.75 A g ⁻¹)	81 %(1000 cycle,3 A g ⁻¹)
Bi+Fe ₃ O ₄ ¹⁷	-1-0V	1 M Na ₂ S _{O₃}	235 F g ⁻¹ (0.2 A g ⁻¹)	72.5 %(5000 cycle,2 A g ⁻¹)

CdS@Bi ₂ Se ₃ ¹⁸	-0.8-0V	1 M NaCl	198 F g ⁻¹ (1 mAh cm ⁻¹)	80 %(2000 cycle,2 A g ⁻¹)
AC-Bi ₂ O ₃ ¹⁹	-1-0V	6 M KOH	252.9 F g ⁻¹ (20 mVs ⁻¹)	59 %(1000 cycle)
This work	0-0.6V	6 M KOH	305.57 F g ⁻¹ (2 A g ⁻¹)	94.12 %(1000 cycle,10 A g ⁻¹)

Tab.S9: Performance Comparison Chart

References

1. X. Yang, P. Deng, D. Liu, S. Zhao, D. Li, H. Wu, Y. Ma, B. Y. Xia, M. Li, C. Xiao and S. Ding, *Journal of Materials Chemistry A*, 2020, **8**, 2472-2480.
2. Y.-f. Fan, Z.-l. Yi, Y. Zhou, L.-j. Xie, G.-h. Sun, Z.-b. Wang, X.-h. Huang, F.-y. Su and C.-m. Chen, *New Carbon Materials*, 2024, **39**, 1015-1026.
3. J. Dai, C. Yang, Y. Xu, X. Wang, S. Yang, D. Li, L. Luo, L. Xia, J. Li, X. Qi, A. Cabot and L. Dai, *Advanced Materials*, 2023, **35**.
4. S. A. Siddiqui, S. Das, S. Rani, M. Afshan, M. Pahuja, A. Jain, D. Rani, N. Chaudhary, Jyoti, R. Ghosh, S. Riyajuddin, C. Bera and K. Ghosh, *Small*, 2023, **20**.
5. Y. Xie, *Fullerenes, Nanotubes and Carbon Nanostructures*, 2021, **30**, 619-625.
6. X. Chen, B. Luo, J. Ding, Q. Yang, D. Xu, P. Zhou, Y. Ying, L. Li and Y. Liu, *Applied Surface Science*, 2023, **609**.
7. J. P. Isaqu, R. Vnekatesan, R. Nagalingam, J. Mayandi and N. Perumal, *International Journal of Energy Research*, 2022, **46**, 11065-11078.
8. L. Gurusamy, S. Anandan, N. Liu and J. J. Wu, *Journal of Electroanalytical Chemistry*, 2020, **856**.
9. R. Mukkabla, M. Deepa and A. K. Srivastava, *Electrochimica Acta*, 2015, **164**, 171-181.
10. H. Qin, Y. Lv, P. Li, M. Xiao, H. Song, Q. Zhang and J. Yang, *New Journal of Chemistry*, 2021, **45**, 21888-21895.
11. T. Yu, Z. Li, S. Chen, Y. Ding, W. Chen, X. Liu, Y. Huang and F. Kong, *ACS Sustainable Chemistry & Engineering*, 2018, **6**, 7355-7361.
12. A. Muthu Kumar, V. Ragavendran, J. Mayandi, K. Ramachandran and K. Jayakumar, *Journal of Materials Science: Materials in Electronics*, 2022, **33**, 9512-9524.
13. H. Lu, Q. Guo, F. Zan and H. Xia, *Materials Research Bulletin*, 2017, **96**, 471-477.
14. J. Wang, C. Zhou, X. Yan, Q. Wang, D. Sha, J. Pan and X. Cheng, *Journal of Materials Science: Materials in Electronics*, 2019, **30**, 6633-6642.
15. A. K. Nayak and T. Gopalakrishnan, *ACS Applied Nano Materials*, 2022, **5**, 14663-14676.
16. H. Zheng, G. Yang, S. Chen and Y. Jia, *ChemElectroChem*, 2017, **4**, 577-584.
17. M. Aghazadeh, I. Karimzadeh and M. R. Ganjali, *Journal of Electronic Materials*, 2018, **47**, 3026-3036.
18. A. C. Mendhe, T. B. Deshmukh, V. Soni, B. R. Sankpal and S.-H. Jang, *Ceramics International*, 2023, **49**, 21978-21987.
19. S. X. Wang, C. C. Jin and W. J. Qian, *Journal of Alloys and Compounds*, 2014, **615**, 12-17.